Supporting Information

Reed *et al.* 10.1073/pnas.0803800105

SI Text

Materials and Methods. ***Preparation.*** Each monkey was given an initial ketamine injection (10–30 mg/kg, intramuscular) for sedation during surgical preparations. Anesthesia was induced with 2–4% halothane gas and maintained with i.v. propofol (10 mg/kg/hr) during surgery. The monkey was secured in a stereotaxic device. Rectal temperature was monitored and maintained at 37–39°C with a servo-controlled heating pad. Paralysis was induced with 1–3 ml of vecuronium bromide and maintained by i.v. vecuronium bromide (0.1–0.3 mg/kg/hr) mixed with 5% dextrose and Lactated Ringer's solution. Once paralyzed, animals were artificially ventilated with a mixture of N_2O: O_2: CO_2 (75: 23.5: 1.5) at a rate sufficient to maintain peak end tidal CO_2 at ≈4%. Paralysis was necessary to keep the hand stable during long stimulus blocks. Depth of anesthesia was monitored by electrocardiogram and electroencephalogram. Supplemental anesthesia (0.3 mg/kg/hr propofol) was provided when needed.

Stimulation procedures. The detailed mapping procedures can be found elsewhere (1, 2). Briefly, we first located responsive regions on the hand for units on each electrode by stimulating lightly with a hand-held probe and listening to the responses on an audio monitor. For well-isolated units, we mapped minimal receptive fields (mRFs) at a finer level by stimulating with graded Semmes-Weinstein filaments (starting with the 10-g filament), finding the threshold, and then drawing mRFs on hand diagrams (3). We marked the estimated excitatory center of the mRF for probe placement. This procedure was conducted at the beginning, end, and periodically throughout the recording experiment. Using hand-plotted mRFs was a practical way to determine probe placement (inside and outside the mRF of reference neurons).

Before stimulation, the fingernails were glued (cyanoacrylic) to Teflon screws that were fixed in plasticine to keep the hand position stable during recording. Adhesive was removed from the fingernails using acetone.

Histology. The myelin-stained sections of flattened cortex were used to help reconstruct the location of the electrodes within S1 by examining the patterns of myelin staining. Area 3b is myelin-rich and stained darkly, and characteristic ''ovals'' representing the face and oral cavity could be identified (4, 5). Electrode depth can be estimated by tracking the appearance and disappearance of electrode tracks across sections. Two primary factors were considered. First, the cortex was cut parallel to the pia, which is not always precisely parallel to the electrode locations. Second, tissue shrinkage and stretching may occur during processing. We estimated this by comparing the observed distance between electrodes across the array to the expected distance (4 mm). By taking these issues into account, we could obtain an approximation of the electrode depth and location.

Data Analysis. ***Spike sorting and data selection.*** Initial spike sorting was performed using the automatic spike classification software available from Cyberkinetics. This method, which uses an adaptation of the Expectation Maximization algorithm with t-distributions, has been shown to perform more reliably than statistical methods that rely on the Gaussian model of waveform variability (6). The automatic nature of the classification and the capacity of the software to be used with data collected from the Bionics recording system made this method of spike sorting the preferred first step. Due to memory limitations and the large amounts of data recorded during an experiment, not all of the possible conditions (recorded over the course of 2 days) were able to be sorted simultaneously with the automatic classification software. However, as mentioned in the text, all of the recordings for a given stimulation protocol were sorted together. For the purpose of the project (beyond the scope of this paper), we wanted to not only compare the responses of the same unit within a given stimulation protocol, but also to compare the responses of the same unit across different stimulation types when the same unit was held. Because the automatic spike sorter program does not designate the units by the same name across multiple recorded files not sorted together, we used the Plexon Offline Sorter program (Plexon Inc., Dallas, TX) to review and sort each recorded file individually. This was necessary to ensure that the same units were compared across stimulus conditions. For example, when more than one unit was recorded on an electrode, the unit called "95b" in recording 1 must be called "95b" in recording 5 to compare those recordings. Plexon Offline Sorter allowed us to swap unit names if necessary and perform semiautomatic sorting (such as Valley-Seeking) if needed to obtain better unit isolation.

In addition, Plexon Offline Sorter allowed us to check the stability of the recordings by viewing the unit clustering in principal component space in three dimensions with the z axis as timestamps (x axis as PC1, y axis as PC2). None of the units included in the analysis were found to drift over time or change unit identities over the course of the stimulation protocol. The manual adjustment capabilities in the Plexon software allowed us to ensure that we used the same populations of units in our control conditions (single-site stimulation) and experimental conditions (nonadjacent dual-site stimulation). We also examined the stability of the recordings by sorting multiple recorded files simultaneously using the Cyberkinetics Matlab-based automatic spike sorting program and viewing the unit isolation in multiple files simultaneously (equivalent to ≈2 h of recording at one time). Units included in the analysis were observed to be stable using both Plexon and Cyberkinetics spike sorter programs.

Spike time synchrony. There are multiple time scales for which temporal correlations can be examined. To assess very precise spike synchrony, small time bins (1–5 ms) have been used; however, such small bins require relatively high spike counts. Coarse temporal correlation is considered at time scales >20 ms. (e.g., refs. 7 and 8) Bin sizes between 1–15 ms are commonly reported (e.g., refs. 8–10). In our case, spike correlation was examined in 700-ms windows divided into 70 bins. We used 10-ms bins because only the brief on and off response transients will peak with firing rates above 100 Hz. This appears to be a reasonable compromise for these data, allowing extraction of the fine temporal correlation especially for the period of relatively low firing during the sustained portion of the stimulus (Fig. 1 and Fig. S3). The peri-stimulus time histograms (PSTH) of spike counts aligned at stimulation onset with 10-ms bins were obtained for each of a pair of neurons:

$$\langle n_{(i)(u)} \rangle = \frac{1}{K} \sum_{k=1}^{K} n_i^{(k)}(u) \qquad [1]$$

where $n_{(i)}^{(k)}(u)$ is the number of spikes per bin in the kth of K total trials. Using the same notation, the contribution to the joint peri-event time histogram (JPETH) of spikes in the kth trial is just the product of the counts in each time bin in the matrix for each neuron in the pair:

$$n_{ij}^{k}(u, v) = n_i^k(u) \cdot n_j^k(v) \quad [2]$$

The average raw JPSTH is obtained by

$$\mathrm{JPSTH}_{\mathrm{raw}} = \langle n_{ij}(u, v) \rangle = \frac{1}{K} \sum_{k=1}^{K} n_{ij}^{(k)}(u, v) \quad [3]$$

The raw JPSTH measures the average incidence of common spike occurrences, but of course, this incidence naturally will be affected by modulation of the discharge rate of either neuron in the pair. The fraction of coincident spikes resulting from such modulation (also known as the shift-predictor) is estimated by calculating the cross-product matrix of the individual peri-event time histograms:

$$\langle \tilde{n}_{ij}(u, v) \rangle = \langle n_i(u) \rangle \langle n_j(v) \rangle \quad [4]$$

In abbreviated notation, the normalized JPSTH was determined by subtracting this shift-predictor from the raw JPSTH and scaling each bin by the square root of the product of the standard deviations from individual neurons:

$$\mathrm{JPSTH}_{\mathrm{normalized}} = \frac{\langle n_{ij} \rangle - \langle \tilde{n}_{ij}(u, v) \rangle}{\sqrt{\langle n_i(u) \rangle (1 - \langle n_i(u) \rangle) \cdot \langle n_j(v) \rangle (1 - \langle n_j(v) \rangle)}} \quad [5]$$

Thus, the normalized JPSTH measures the probability of coincident spikes in a pair of neurons corrected for overall modulation of discharge rates; the values are treated as correlation coefficients, ranging from -1 to $+1$ (10).

The JPSTH matrix represents time from earlier in the lower left to later in the upper right; the bins along this main diagonal measure coincidences with 0 time lag (Fig. 1*C*). The JPSTH can be summarized in two additional plots. First, the time-averaged cross-correlogram is computed by summing the JPSTH bins parallel to the main diagonal; the cross-correlogram measures the average positive or negative correlation across the entire interval of analysis (Fig. 1*C*). Second, the coincidence histogram (data not shown) represents the coincident or near-coincident firing of the cells time-locked to the event on which the PETH are aligned. Although the dynamics of the correlation are not analyzed here, examination of the JPSTH revealed that the correlated spike times occur during the sustained portion of the stimulus-driven activity, rather than at the transient responses to stimulus onset and removal. The spike timing coincidence will be examined elsewhere.

To test the reliability of the normalized JPSTH, we repeated the JPSTH calculation on two sets of spike trains in which no correlation should be present. In the first case, the spike train variability was preserved, whereas in the second case the spike train variability was derived from a nonhomogeneous Poisson process. The first was the shuffled JPETH generated by shuffling the order of the trials for one of each pair of neurons. It is important to emphasize that the trial-by-trial variability present in the normalized JPETH is preserved within the shuffled JPETH even if no correlation should be observed. Only pairs showing a normalized JPSTH correlation value significantly larger than the shuffled JPSTH were considered for further analysis. In practice, a bootstrapping (5,000 iterations) procedure was used to test each correlation value against the distribution of the entire population of shuffled correlation values. Only the pairs for which the correlation value exceeded two times the standard deviation over the mean of the bootstrapped distribution were considered significant.

Firing rate spike density function. Peak firing rate of individual neuron-units was determined from spike density functions. A spike density function was produced by convolving the spike train from each trial with a function resembling a postsynaptic potential specified by τ_g, the time constant for the growth phase, and τ_d, the time constant for the decay phase as $R(t) = (1 - \exp(-t/\tau_d) \cdot \exp(-t/\tau_d)$. Based on physiological data from excitatory synapses, τ_g was set to 1 ms (e.g., refs. 11 and 12). We set τ_d to 5 ms (11–14) rather than the commonly used 20 ms because the transient nature of the on and off responses in primary somatosensory neurons was excessively smoothed with a decay constant of 20 ms. Other stimulus conditions in the same monkeys included dual-site stimulation delivered at temporal offsets of 10 and 30 ms (results will be presented elsewhere); therefore, we selected a smaller value for τ_d that best fit the data.

We visualized the peak firing rates across the sampled neurons in the 100-electrode array by creating a color map in Matlab. In some cases, to view the extent of high and low firing rates, we converted the firing rate values to logarithmic values. These graphs are for visualization purposes only.

1. Merzenich MM, Kaas JH, Sur M, Lin CS (1978) Double representations of the body surface within cytoarchitectonic areas 3b and 1 in ''SI'' in the owl monkey (*Aotus trivirgatus*). *J Comp Neurol* 181:41–74.
2. Nelson RJ, Sur M, Felleman DJ, Kaas JH (1980) Representations of the body surface in postcentral parietal cortex of Macaca fascicularis. *J Comp Neurol* 192:611–643.
3. Jain N, Qi HX, Kaas JH (2001) in *Progress in Brain Research*, ed Nicolelis MAL, (Elsevier Science, Amsterdam) Vol 130, pp 1–10.
4. Jain N, Catania KC, Kaas JH (1998) A histologically visible representation of the fingers and palm in primate area 3b and its immutability following long-term deafferentations. *Cereb Cortex* 8:227–236.
5. Jain N, Qi HX, Catania KC, Kaas JH (2001) Anatomical correlates of the face and oral cavity representations in the somatosensory area 3b of monkeys. *J Comp Neurol* 429:455–468.
6. Shoham S, Fellows MR, Normann RA (2003) Robust, automatic spike sorting using mixtures of multivariate t-distributions. *J Neurosci Methods* 127:111–122.
7. Oram MW, Hatsopoulos NG, Richmond BJ, Donoghue JP (2001) Excess synchrony in motor cortical neurons provides redundant direction information with that from coarse temporal measures. *J Neurophysiol* 86:1700–1716.
8. Vaadia E, *et al.* (1995) Dynamics of neuronal interactions in monkey cortex in relation to behavioural events. *Nature* 373:515–518.
9. Benda J, Longtin A, Maler L (2006) A synchronization-desychronization code for natural communication signals. *Neuron* 52:347–358.
10. Narayanan NS, Laubach M (2006) Top-down control of motor cortex ensembles by dorsomedial prefrontal cortex. *Neuron* 52:921–931.
11. Mason A, Nicoll A, Stratford K (1991) Synaptic transmission between individual pyramidal neurons of the rat visual cortex *in vitro*. *J Neurosci* 11:72–84.
12. Moore CI, Nelson SB (1998) Spatio-temporal subthreshold receptive fields in the vibrissa representation of rat primary somatosensory cortex. *J Neurophysiol 80:2882-*2892.
13. Veredas FJ, Vico FJ, Alonso JM (2005) Factors determining the precision of the correlated firing generated by a monosynaptic connection in the cat visual pathway. *J Physiol 567* 3:1057–1078.
14. Steinmetz PN *et al*. (2000) Attention modulates synchronized neuronal firing in primate somatosensory cortex. *Nature* 404:187–190.

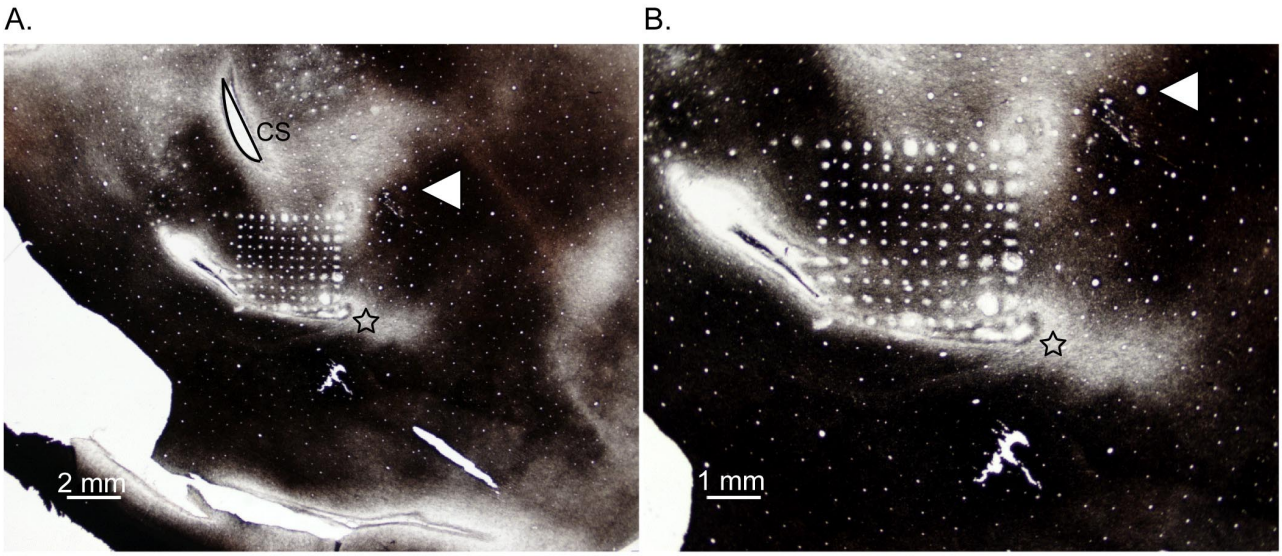

Fig. S1. Illustration of tissue quality with use of the 100-electrode array. The damage produced by inserting the array appears to be minimal in most cases, but tears in the tissue caused by array removal and tissue processing are common and did occur for both of the presented cases. Photomicrographs were adjusted for brightness and contrast in Adobe Photoshop CS but were not altered in any other way. Graphics and text were added in Adobe Illustrator 10. Medial is up and rostral is to the right in *A* and *B*. White arrowheads mark matching blood vessels and the stars indicate approximately matched sites near the lateral sulcus. (*A*) The individual electrode sites are visible in this section at 0.5 × magnification (section 13) from one owl monkey in which the 100-electrode array was acutely implanted and removed after recording for >2 days. CS indicates the location of the central sulcus. (*B*) The same section in *A* is shown at 1× magnification to show the detail of the electrode tracks. We find that the majority of the tissue damage comes from removing the electrode array from the brain before perfusion and from processing the tissue.

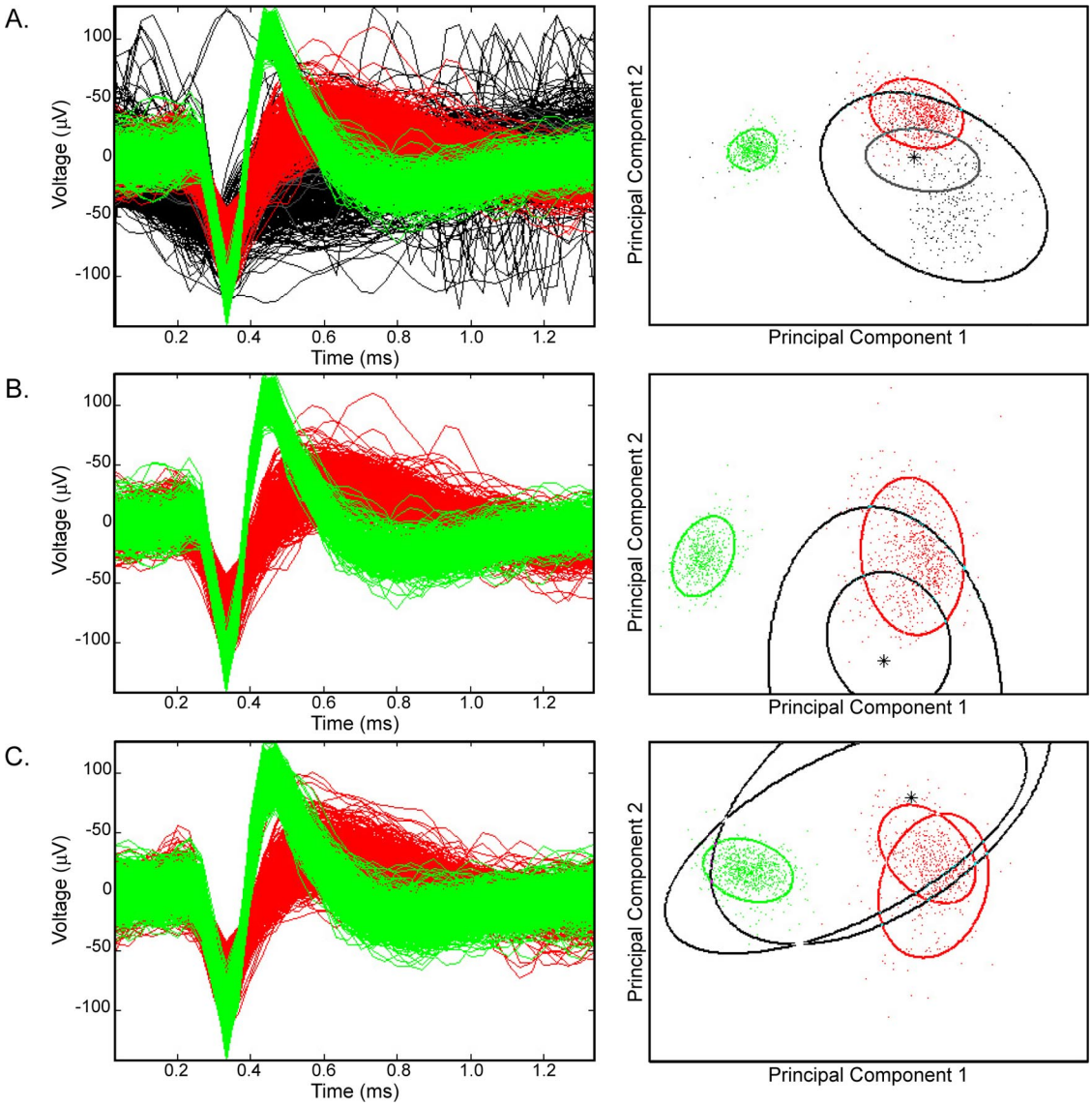

Fig. S2. Examples of spike sorting quality. (*A*) The left plot shows waveforms recorded from electrode 95 in monkey 2 from the Cyberkinetics Matlab-based automatic spike sorting program during stimulation on distal D2. The 539 waveforms classified as a single unit (green) were distinguishable from other waveforms. The black waveforms are classified as noise by the Matlab-based automatic spike sorter program. We considered the red unit a multiunit due to the lack of separation from the background noise spikes. The right plot of the first and second principal components (PC1 and PC2) shows separate clustering of the single unit (green) from the background spikes (black). Because it was possible to record from multiple units per electrode, we examined the recorded files individually using Plexon Offline Sorter to ensure that the appropriate units were compared across recordings. In most cases, spikes that belong to one unit but are counted as ''noise'' in the automatic spike sorter can be added to the appropriate unit using the Plexon program. See large amplitude ''noise'' waveforms and spikes within the green cluster. (*B*) The same plot style and units in *A* are shown after the ''erase noise'' feature is used in the Matlab-based automatic spike sorting program to focus on the spikes from the green unit and the cluster separation. When two units were recorded simultaneously from one electrode, we only selected one unit per electrode for synchrony analysis, choosing single units over multiunits. In this case, we chose the single unit shown in green (designated as 95b). (*C*) One way to view the stability of the recordings and unit designations is to show the appearance of waveforms and clusters across a series of stimulations. This function cannot be performed using the Plexon spike sorting program unless all of the stimulations are recorded in the same file. The recordings for single-site stimulation on D2 and D4, simultaneous stimulation on D2 and D4, and temporally offset stimulation on D2 and D4 (data not presented here) encompassed 620 trials recorded over 79 min. The plot style is the same as *B* with ''noise'' spikes hidden to focus on the isolation of single unit 95b (green) over the time course of the stimulus series.

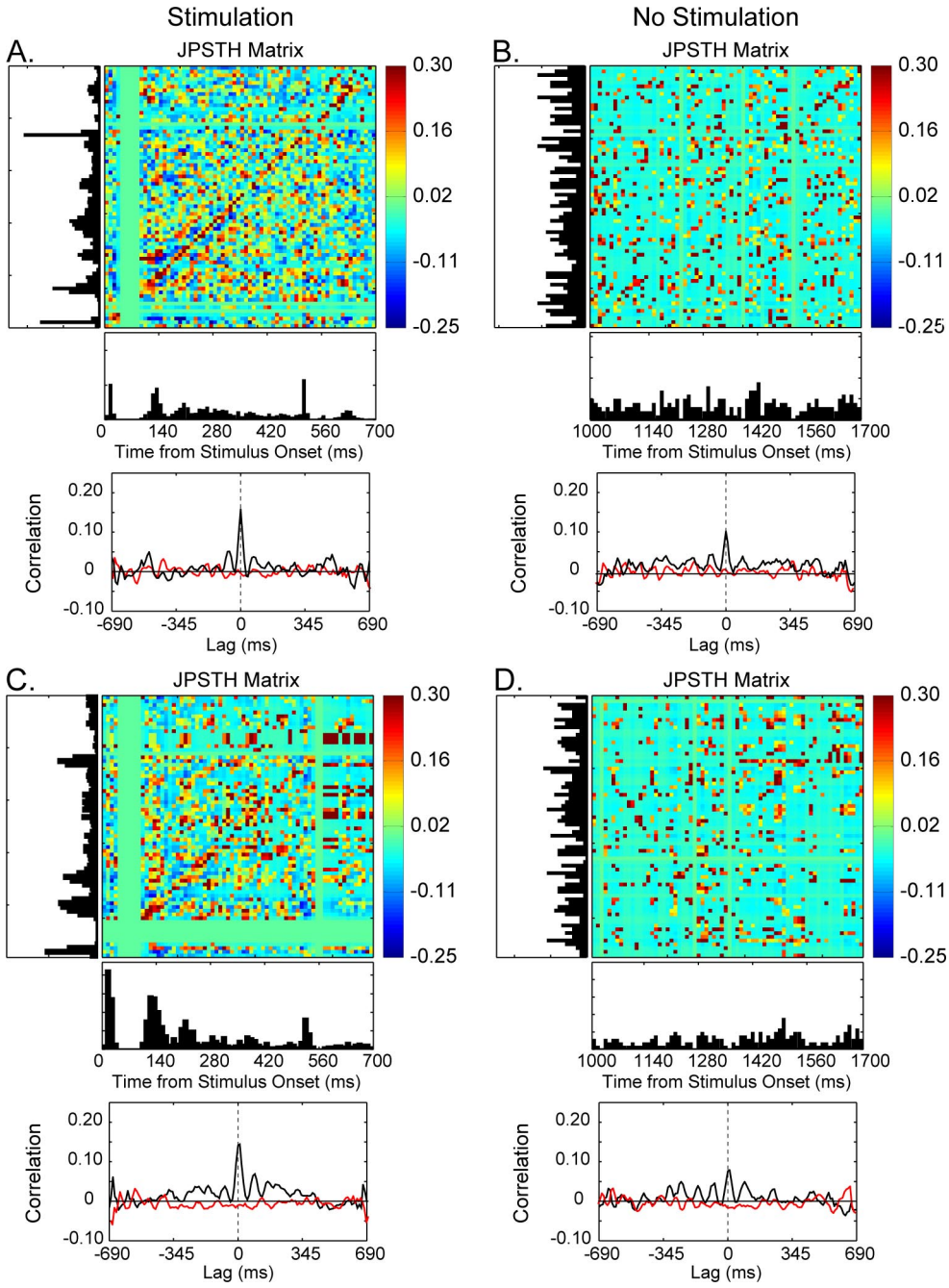

Fig. S3. Examples of spike time synchrony during trials with or without tactile stimulation. The left column includes results during stimulation with the 500-ms indentation from 0 to 700 ms. The right column includes results during the stimulus-off periods from the same trials from 1000 to 1700 ms. The same conventions as Fig. 1 are used for the JPSTH plot. (*A*) The JPSTH matrix and associated cross-correlation histogram are shown for multiunits 5a and 15a from monkey 1 during 100 trials of dual-site stimulation on palm sites PTh and P1. The normalized peak correlation is 0.16, centered on 0 ms. Unit 5a has 1439 spikes, and unit 15a has 2359 spikes. (*B*) The JPSTH and cross-correlation histogram are shown for the same units as A during the portion of the trials when the tactile probes were off the skin. Each trial contained a 2-s interstimulus interval when the probes were not touching the skin. The normalized peak correlation is 0.11, centered on 0 ms. Unit 5a has 246 spikes, and unit 15a has 419 spikes. (*C*) The JPSTH and cross-correlation histogram are shown for single units 85a and 95b from monkey 2 during 100 trials of dual-site stimulation on digit sites distal D2 and D4. The normalized peak correlation is 0.14, centered on 0 ms. Unit 85a has 784 spikes, and unit 95b has 790 spikes. (*D*) The JPSTH and cross-correlation histogram are shown for the same units as C during the portion of the trials when the tactile probes were off the skin. The normalized peak correlation is 0.08, centered on 0 ms. Unit 85a has 200 spikes, and unit 95b has 386 spikes. Because the spike numbers were typically very low when no tactile stimulation was provided, we did not analyze the correlations from these data. The presence of these correlations in the absence of a driving stimulus confirms that the peak correlations measured and interpreted did not result from spike coincidence due to the brief and extreme changes in firing rate during initiation and removal of stimulation.